Scalable and template-free production of mesoporous calcium carbonate and its potential to formaldehyde adsorbent

Scalable and template-free production of mesoporous calcium carbonate and its potential to formaldehyde adsorbent

Shinya Yamanaka*[1], Takahiro Oiso [2], Yuya Kurahashi [2], Hiroya Abe[3], Kenji Hara[4], Toshiyuki Fujimoto [1] and Yoshikazu Kuga [1]

[1] College of Environmental Technology, Muroran Institute of Technology, Mizumoto-cho 27-1, Muroran 050-8585, Japan

[2] Division of Applied Sciences, Muroran Institute of Technology, Mizumoto-cho 27-1, Muroran 050-8585, Japan

[3] Joining and Welding Research Institute, Osaka University, 11-1 Mihogaoka, Ibaraki, Osaka 567-0047, Japan

[4] Catalysis Research Center, Hokkaido University, Kita 21 Nishi 10, Kita-ku, Sapporo, Hokkaido 001-0021, Japan

* Corresponding author. Tel.: +81 143 46 5747; fax: +81 143 46 5701.

E-mail address: syama@mmm.muroran-it.ac.jp (S. Yamanaka).

Abstract: Here we report a scalable and template-free production strategy in the synthesis of a mesoporous calcium carbonate, which undergoes self-assembled nanostructure formation through a temperature-induced aggregation and polymorphic transformation of the colloids. The specific surface area and pore size distribution of resulting mesoporous calcium carbonate are clearly different depending on the aging temperature. The specific surface area and average pore size for aging temperature of 293 K are 207.3±9.8 m^2/g and 8.8±0.6 nm, respectively, and 65.1±10.1 m^2/g and 19.9±2.6 nm at 473 K. Additionally, we apply the mesoporous calcium carbonate powder to formaldehyde vapor adsorbent. We measure the adsorbed amount of gaseous formaldehyde and find that the vaterite-rich powder has larger adsorption per unit area than the calcite-rich one.

Keywords: Mesoporous calcium carbonate, vaterite, colloid processing, self-assembled nanostructure, formaldehyde adsorbent

1. Introduction

Calcium carbonate is one of the most abundant minerals and is widely used in industry as a raw material for cement, paper coating, and medicines, among others. The organization of its primary building units into hollow and porous superstructures is of considerable interest due to their promising applications in controllable release and encapsulation of drugs [Sukhorukov et al. 2004; Wei et al. 2008; Fujiwara et al. 2010], catalyst support [García-Mota et al. 2011], gas adsorbent [Zhao et al. 2011], as well as biomimetics [Addadi et al. 2003; Faatz et al. 2004; Xu et al. 2007]. Thus far, there have been two main processes capable of producing ordered superstructures of calcium carbonate. One is surface crystallization on templates [Walsh and Mann 1995; Tomioka et al. 2011], and the other is non-classical crystallization via colloidal intermediates [Cölfen and Mann 2003]. Nevertheless, large-scale production involving porous superstructure formation of calcium carbonate remains challenging. Organized assemblies or soft templates have been commonly used for polymorph-controlled synthesis of calcium carbonate crystals [Qi et al. 2002; Yang et al. 2003]. Besides conventional crystallizations, ordered superstructures (i.e. mesocrystals) can be assembled from nanoscopic building units, in what is known as "non-classical" crystallization [Jongen et al. 2000; Cölfen and Mann 2003; Wang et al. 2005]. In this case, a soluble additive with well-defined concentration mediates the mesoscale transformation. These researches have not only offered important contributions to an understanding of biomineralization, also opened up the promising applications.

Various porous materials with huge specific surface areas such as activated carbon [Rong et al. 2003; Lee et al. 2010; Carter et al. 2011; Wen et al. 2011], silica [Srisuda and Virote. 2008], and hydroxyapatite [Kawai et al. 2006] have received much attention as

highly effective adsorbents for formaldehyde vapor. Formaldehyde, which is one of the most representative volatile organic compound, is highly toxic to humans. In our previous work [Yamanaka et al. 2013], we reported effective uses for discarded scallop shells as a formaldehyde adsorbent. We found that the specific surface area of the shell particles was positively correlated with the adsorbed amount of formaldehyde vapor.

We now demonstrate how mesoporous calcium carbonate powder applies to formaldehyde vapor adsorbent. We present a scalable production system of mesoporous calcium carbonate by means of an industrial carbonation process. In this process, self-assembled nanostructure formation takes place via Brownian aggregation of nanoscale building units in a colloidal intermediate dispersion. We then investigate the effect of thermal energy on the self-assembled pore structure and crystal polymorphs.

2. Experimental procedure

2.1 Materials and synthesis of porous calcium carbonate

Calcium hydroxide was purchased from Nacalai Tesque Inc., and ethylene glycol and ethanol were purchased from Kanto Chemical Co., Inc. Calcium carbonate was prepared by carbonation of calcium hydroxide in ethylene glycol–ethanol organic solvent mixture [Yasue et al. 1985]. Calcium hydroxide (25.0 g) was mixed with the mixture of ethylene glycol and ethanol (3:7 by weight to yield a total weight of 475.0 g) in the crystallizer. Calcium hydroxide reacted with CO_2 introduced from the bottom of the crystallizer, in which the stirring was conducted at the rate of 400 rpm. CO_2 was blended with N_2 at the concentration of 30 vol%, and the flow rate of CO_2 was 0.3 *l*/min. The carbonation reaction temperature was controlled at 293 K using a water bath. After the carbonation, the

suspension was centrifuged at 3,500 rpm for 30 min. The transparent supernatant was aged at a predetermined temperature. The subsequent treatment deals with the unnecessary organic solvent. The cloudy suspension was washed twice with ethanol to eliminate the excess ethylene glycol. The suspension was then centrifuged at 3,500 rpm for 20 min. The supernatant was then discarded, and the residue was dried in vacuum for 12 h. The resulting dry powder was used in the measurements.

2.2 Characterization

The specific surface area of the resulting samples was determined by nitrogen gas adsorption based on the multi-point BET method. Pore size distribution was determined by the BJH method. Both analyses were conducted on Autosorb-1-c/MK2 (Qantachrome, USA). In the BET and pore size distribution measurements, the samples were degassed for 2 h at 473 K under a vacuum to remove adsorbed solvent molecules. To determine the crystal structure, X-ray diffraction (XRD, MultiFlex, Rigaku, Japan) powder patterns of the samples were obtained with Cu Kα radiation (40 kV, 40 mA). SEM studies were performed using a JEOL JSM-6380A. The TEM image and selected area electron diffractions (SAEDs) were taken on a JEM-2100F operated at 200 kV after the sample powder was transferred onto a carbon-coated TEM grid.

2.3 Formaldehyde adsorption

The amount of adsorbed formaldehyde was measured by the constant volume method at 293 K, using a home-built vacuum line system. The procedure for the adsorption test is described in detail elsewhere [Yamanaka et al. 2013]. Briefly, the samples (0.2 g) were

precisely weighed in a bag made of non-woven fabric. Samples were placed into a cross-shaped cell and dried in vacuum overnight. Formaldehyde vapor (1866 Pa of total pressure) was introduced into the cell connected to the vacuum line. After the total pressure was reduced to 1600 Pa for adsorbing the vapor, we increased the total pressure to 1866 Pa, and this sequence was repeated until the system achieved equilibrium. The pressure difference before and after adsorption was then measured. Mole fraction of formaldehyde in the vapor phase is not equal that in the liquid phase because formaldehyde is a polar organic compound. Then, the amount of substance per unit sample weight was calculated from the equation of state for an ideal gas with an added correction factor of 0.27 [Yamanaka et al. 2013], and the amount of substance per unit sample area was obtained from its specific surface area.

3. Results and discussion

In an industrial production system, calcium carbonate is produced on a large scale by carbonation of calcium hydroxide in water. We believe that our synthesis method is easily applied to an industrial system because we just switch the solvent from water to the organic solvent mixture. A schematic description of production of porous calcium carbonates is given in **Fig. 1**. We prepared a transparent dispersion of calcium carbonate nanoparticles (Fig. 1a), the starting liquid material for porous calcium carbonate particles, by carbonation of calcium hydroxide in ethylene glycol–ethanol organic solvent mixture (see section 2.1). Prepared liquid is a colloidal dispersion because it is transparent but exhibits the Tyndall effect. The solid fraction of the dispersion was calculated from the weight loss at 773 K using thermogravimetric-differential thermal analysis (TG-DTA; Seiko Instruments Exstar

6200N, 50 ml/min nitrogen flow, 10 K/min ramp). The solid fraction was 5.5±0.2 mass%, with a yield of about 80%. The dispersion was then aged for a predetermined time to provide a thermal energy that leads to Brownian aggregation of the calcium carbonate nanoparticles via a gel (Fig. 1b). The organized pore structure of the calcium carbonate particles was controlled by aging temperature, because the Brownian aggregation rate and structural phase transition depend on temperature. During the aging process, the time for a transparent dispersion to become cloudy sol was 1 hour at 353 K, and 2 days at 293 K, for example.

We present first the characterization results for the porous calcium carbonate particles. The particle properties are summarized in **Table 1**. The specific surface area and pore size distribution highly differed according to the aging temperature. The specific surface area and average pore size for aging temperature of 293 K were 207.3±9.8 m^2/g and 8.8±0.6 nm, respectively, and 65.1±10.1 m^2/g and 19.9±2.6 nm at 473 K (**Fig. 2a, e**, and see Table 1). Figure 1c shows typical SEM images of the porous calcium carbonate particles obtained for aging temperatures of 293 K and 473 K. At low aging temperature, the particles form ellipsoidal structure, and dumbbell or rod-like structure at higher temperature. The major and minor axis size for the ellipsoidal shape of calcium carbonate were 0.63±0.07 and 0.33±0.04 μm, respectively, and 1.45±0.36 and 0.40±0.07 μm for the dumbbell-like shape (see Table 1).

The peak positions of XRD profiles agree with those of the calcite (ICDD#05-0586) and/or vaterite (ICDD#33-0268) crystal for all samples (the corresponding results of the XRD profiles are shown in **Fig. 3**). The intensities of the calcite diffraction peaks decrease with increasing aging temperature, as the vaterite peaks rose up. The ratio of vaterite to

calcite crystal (f_V) calculated from Rao's equation below [Rao 1973].

$$f_V = \frac{I_{100V} + I_{112V} + I_{114V}}{I_{100V} + I_{112V} + I_{114V} + I_{104C}}$$

The subscript V and C indicate vaterite and calcite, respectively. The ratio of vaterite (f_V) increased with temperature (see Table 1). TEM observation revealed that the ellipsoidal structure was composed of minute calcite particles (Fig. 2b–d), whereas dumbbell-like structure had hierarchical vaterite framework (Fig. 2f–h).

Generally, three types of crystalline calcium carbonate (calcite, aragonite, and vaterite) are crystallized from amorphous calcium carbonate (ACC) [Addadi et al. 2003; Cölfen and Mann 2003; Faatz et al. 2004]. In the carbonation reaction, the initially formed ACC is immediately transformed into vaterite and calcite [Wei et al. 2003; Han et al. 2005]. Recently, Rodriguez-Blanco et al. reported the kinetics and mechanism of ACC crystallization and found that the calcite was formed via dissolution of vaterite and subsequent reprecipitation [Rodriguez-Blanco et al. 2011]. Thus the solubility of calcium carbonate is crucial for the transformation [Hadiko et al. 2005]. Naka et al. successfully prepared stable vaterite particles by a delayed addition of polyacrylic acid (PAA) after the crystallization of calcium carbonate in the aqueous solution [Naka et al. 2006]. They concluded the vaterite particles were stable in consequence of binding PAA with calcium ions, which prevented phase transformation into calcite. Additionally, the solubility of calcium carbonate decreased in the mixture of ethylene glycol and water [Flatena et al. 2010] compared with pure water. Because the carbonation process in this study contains little water, the dissolution of vaterite, i.e. transformation into calcite should not occur. The

above discussion and the observation results indicate that there are two transformation routes: one is transformation from amorphous to calcite, the other is into vaterite. Figures 1d–f schematically illustrate the effect of aging temperature on the formation of porous calcium carbonate. As previously mentioned, the primary size of nanoparticles in the colloidal dispersion aggregated together was associated with the weak repulsive force (Fig. 1d), because electrostatic interactions are negligible in such a relatively low dielectric constant medium [Israelachvili 1992]. At the same time, phase transition from unstable amorphous to stable calcite or metastable vaterite was also taking place (Fig. 1e). The colloidal particles undergo more preferable self-assembly to form ellipsoidal or dumbbell-shape aggregated structures, resulting from the reduction of the surface free energy [Guo et al. 2010]. When the system temperature is high, the metastable vaterite particles are formed, which drives them into forming layered stacking structures (Fig. 1f). In another one of our experiments, where the aging temperature was set to 293, 313, 333, 353, and 473 K, the vaterite-rich particles increased with the aging temperature as shown in **Fig. 4a**.

In our previous work using scallop shells (calcite) [Yamanaka et al. 2013], we demonstrated formaldehyde adsorption for nanosized shell particles that were prepared by planetary ball milling and subsequent water addition. The largest specific surface area for the ground shell was 54.4 m^2/g, and the maximum adsorbed amount of formaldehyde vapor was 1.1 mg/g. This value was a significant improvement in the adsorption amount compared to the feed shell particles (0.1 mg/g). We then reported that the specific surface area of the scallop shell particles was positively correlated with the adsorbed amount of formaldehyde vapor per unit weight of the shell particle.

In this work, we have successfully prepared mesoporous calcium carbonate with a large specific surface area of 207.3 m^2/g (the ratio of vaterite crystal, f_V, was 0.11). The adsorbed amount of formaldehyde per unit weight was 8.2 mg/g, indicating specific surface area had a large influence on the formaldehyde adsorption, as expected. While using the vaterite-rich calcium carbonate (f_V was 0.88, and specific surface area was 65.1±10.1 m^2/g), the adsorbed amount was 6.7 mg/g, which was approximately 6 times higher per unit weight, although its specific surface area was approximately equal to that of above ground scallop shell particles. We now focus on the adsorbed amount of formaldehyde per unit area (see section 2.3). As shown in **Fig. 4b**, the adsorbed amount per unit area increased with increasing ratio of vaterite crystal. The vaterite-rich sample (f_V=0.88, 0.11 mg/m^2) had ca. 4 times higher adsorption capacity per unit area than the calcite-rich one (f_V=0.11, 0.03 mg/m^2). It should be noted that the vaterite has a structure that enables it to adsorb formaldehyde easily. We measured FTIR spectra for calcite-rich and vaterite-rich calcium carbonate before and after formaldehyde adsorption (data not shown). We did not detect any differences other than the different polymorphs of calcium carbonate. This observation makes it difficult to explain the contributions of surface structure on the adsorption capacity. The modeled surface energies of vaterite are in the range 0.62–1.58 J/m^2 for the anhydrous surface, which is higher than that of calcite (104) surface (0.59 J/m^2) [de Leeuw and Parker 1998]. The favorable structure for gas adsorption reflects the surface energy and the thermodynamic stability of the polymorphs. We believe that the porous calcium carbonate presented here may also be a promising drug carrier material or template, due to its characteristic superstructure and very high specific surface area.

4. Conclusion

We have demonstrated a scalable production method for mesoporous calcium carbonate of which maximum specific surface area was 207.3 m^2/g. We have also assessed its potential use as a formaldehyde vapor adsorbent. The vaterite was an appropriate polymorph of calcium carbonate in formaldehyde vapor adsorption compared to the calcite.

Acknowledgment

We thank Prof. Jusuke Hidaka at Doshisha University for technical comment and assistance. This work was supported by a Grant-in-Aid for Young Scientists (B) (No. 24710074) and a Grant-in-Aid for Scientific Research (C) (No. 22560812) of the Japan Society for the Promotion of Science, by the Cooperative Research Program of Catalysis Research Center, Hokkaido University, and performed under the Cooperative Research Program of Institute for Joining and Welding Research Institute, Osaka University.

References

Addadi L, Raz S, Weiner S (2003) Taking advantage of disorder: Amorphous calcium carbonate and its roles in biomineralization. Adv Mater 15: 959-970.

Carter EM, Katz LE, Speitel Jr GE, Ramirez D (2011) Gas-phase formaldehyde adsorption isotherm studies on activated carbon: correlations of adsorption capacity to surface functional group density. Environ Sci Technol 45: 6498–6503.

Cölfen H, Mann S (2003) Higher-order organization by mesoscale self-assembly and transformation of hybrid nanostructures. Angew Chem Int Ed 42: 2350-2365.

de Leeuw NH, Parker SC (1998) Surface structure and morphology of calcium carbonate polymorphs calcite, aragonite, and vaterite: An atomistic approach. J Phys Chem B 102: 2914-2922.

Faatz M, Grohn F, Wegner G (2004) Amorphous calcium carbonate: Synthesis and potential intermediate in biomineralization. Adv Mater 16: 996-1000.

Flatena EM, Seierstenb M, Andreassen JP (2010) Induction time studies of calcium carbonate in ethylene glycol and water. Chem Eng Res Des 88: 1659-1668.

Fujiwara M, Shiokawa K, Araki M, Ashitaka N, Morigaki K, Kubota T, Nakahara Y (2010) Encapsulation of proteins into $CaCO_3$ by phase transition from vaterite to calcite. Cryst Growth Des 10: 4030-4037.

García-Mota M, Gómez-Díaz J, Novell-Leruth G, Vargas-Fuentes C, Bellarosa L, Bridier B, Pérez-Ramírez J, López N (2011) A density functional theory study of the 'mythic' Lindlar hydrogenation catalyst. Theor Chem Acc 128: 663-673.

Guo XH, Deng YH, Tu B, Zhao DY (2010) Facile synthesis of hierarchically mesoporous silica particles with controllable cavity in their surfaces. Langmuir 26: 702-708.

Hadiko G, Han YS, Fuji M, Takahashi M (2005) Synthesis of hollow calcium carbonate particles by the bubble templating method. Mater Lett 59: 2519-2522.

Han YS, Hadiko G, Fuji M, Takahashi M (2005) Effect of flow rate and CO_2 content on the phase and morphology of $CaCO_3$ prepared by bubbling method. J Crystal Growth 276: 541-548.

Israelachvili JN (1992) Intermolecular and surfaces forces, 2nd edn. Academic Press, London, U.K.

Jongen N, Bowen P, Lemaître J, Valmalette J, Hofmann H (2000) Precipitation of self-organized copper oxalate polycrystalline particles in the presence of hydroxypropylmethylcellulose (HPMC): Control of morphology. J Colloid Interface Sci 226: 189-198.

Kawai T, Ohtsuki C, Kamitakahara M, Miyazaki T, Sakaguchi Y, Konagaya S (2006) Removal of formaldehyde by hydroxyapatite layer biomimetically deposited on polyamide film. Environ Sci Technol 40: 4281-4285.

Lee KJ, Shiratori N, Lee GH, Miyawaki J, Mochida I, Yoon SH, Jang J (2010) Activated carbon nanofiber produced from electrospun polyacrylonitrile nanofiber as a highly efficient formaldehyde adsorbent. Carbon 48: 4248−4255.

Mullin JW (2001) Crystallization, 4th edn. Butterworths-Heinemann, Oxford, U.K.

Naka K, Huang SC, Chujo Y (2006) Formation of stable vaterite with poly(acrylic acid) by the delayed addition method. Langmuir 22: 7760-7767.

Qi L, Li J, Ma J (2002) Biomimetic morphogenesis of calcium carbonate in mixed solutions of surfactants and double-hydrophilic block copolymers. Adv Mater 14: 300-303.

Rao MS (1973) Kinetics and mechanism of the transformation of vaterite to calcite. Bull Chem Soc Jpn 46: 1414-1417.

Rodriguez-Blanco JD, Shaw S, Benning LG (2011) The kinetics and mechanisms of amorphous calcium carbonate (ACC) crystallization to calcite, via vaterite. Nanoscale 3: 265-271.

Rong HQ, Ryu ZY, Zheng JT, Zhang YL (2003) Influence of heat treatment of rayon-based activated carbon fibers on the adsorption of formaldehyde. J Colloid Interface Sci 261: 207-212.

Srisuda S, Virote B (2008) Adsorption of formaldehyde vapor by amine-functionalized mesoporous silica materials. J Environ Sci 20:379–384

Sukhorukov GB, Volodkin DV, Günther AM, Petrov AI, Shenoy DB, Mohwald H (2004) Porous calcium carbonate microparticles as templates for encapsulation of bioactive compounds. J Mater Chem 14: 2073-2081.

Tomioka T, Fuji M, Takahashi M, Takai C, Utsuno M (2011) Hollow structure formation mechanism of calcium carbonate particles synthesized by the CO_2 bubbling method. Cryst Growth Des 12: 771-776.

Walsh D, Mann S (1995) Fabrication of hollow porous shells of calcium carbonate from self-organizing media. Nature 377: 320-323.

Wang T, Cölfen H, Antonietti M (2005) Nonclassical crystallization: Mesocrystals and morphology change of $CaCO_3$ crystals in the presence of a polyelectrolyte additive. J Am Chem Soc 127: 3246-3247.

Wei H, Shen Q, Zhao Y, Wang DJ, Xu DF (2003) Influence of polyvinylpyrrolidone on the precipitation of calcium carbonate and on the transformation of vaterite to calcite. J Crystal

Growth 250: 516-524.

Wei W, Ma GH, Hu G, Yu D, Mcleish T, Su ZG., Shen ZY (2008), Preparation of hierarchical hollow $CaCO_3$ particles and the application as anticancer drug carrier. J Am Chem Soc 130: 15808-15810.

Wen Q, Li C, Cai Z, Zhang W, Gao H, Chen L, Zeng G, Shu X, Zhao Y (2011) Study on activated carbon derived from sewage sludge for adsorption of gaseous formaldehyde. Bioresour Technol 102: 942-947.

Xu AW, Ma Y, Cölfen H (2007) Biomimetic mineralization. J Mater Chem 17: 415-449.

Yamanaka S, Suzuma T, Fujimoto T, Kuga Y (2013) Production of scallop shell nanoparticles by mechanical grinding as a formaldehyde adsorbent. J Nanoparticle Res 15, 1573.1-8.

Yang D, Qi L, Ma J (2003) Well-defined star-shaped calcite crystals formed in agarose gels. Chem Commun 21: 1180-1181.

Yasue T, Mamiya A, Fukushima T, Arai Y (1985) Synthesis and characteristics of amorphous calcium carbonate in ethanol. Gypsum & Lime 198: 245-252.

Zhao Z, Zhang L, Dai H, Du Y, Meng X, Zhang R, Liu Y, Deng J (2011) Surfactant-assisted solvo- or hydrothermal fabrication and characterization of high-surface-area. Microporous Mesoporous Mater 138: 191-199.

Figure captions

Fig. 1 (a) Starting liquid material for porous calcium carbonate particles. (b) After the dispersion was aged for a predetermined amount of time, it became cloudy via a gelling state. (c) Typical SEM images of the porous calcium carbonate particles obtained by aging at 293 K and 473 K. The scale bar is 1 μm. (d, e, and f) Schematic illustration of the effect of aging temperature on the formation process of porous calcium carbonate. (d) Primary size of nanoparticles in the colloidal dispersion. (e) Primary particles are aggregated together due to the weak repulsive force; while phase transition from unstable amorphous to stable calcite or metastable vaterite occurs. (f) Finally, the colloidal particles undergo a more preferable self-assembly to form ellipsoidal or dumbbell-shape aggregated structures.

Fig. 2 Some features of the samples obtained by aging at 293 K (a–d), and 473 K (e–h). (a) BJH pore size distributions measured from nitrogen isotherm plots, (b) TEM image, (c) magnified image, and (d) SAED patterns obtained by electron diffraction study. (e) BJH pore size distributions, (f) TEM image, (g) magnified image, and (h) SAED patterns of the particle.

Fig. 3 Typical XRD patterns of the prepared particles. The upper one is a sample obtained at 473 K, and the lower one at 293 K aging temperature. The crystallite size was 15 nm for (104) calcite, and 14 nm for (112) vaterite. The values almost coincide with the primary particle size from each TEM image (see Fig. 2c and g). The crystallite size was calculated from the full width at half maximum (FWHM) of the corrected diffraction profile. A Pseudo-Voigt fitting was conducted to obtain the FWHM for the (104) calcite and (112)

vaterite diffraction.

Fig. 4 (a) The effect of the aging temperature on the crystal structure of porous calcium carbonate. The ratio of vaterite crystal was calculated from Rao's equation [Rao 1973]. (b) Relation between the ratio of vaterite phase and adsorbed amount of formaldehyde per unit area for formaldehyde concentration of 1560 mg/m^3.

Fig. 1

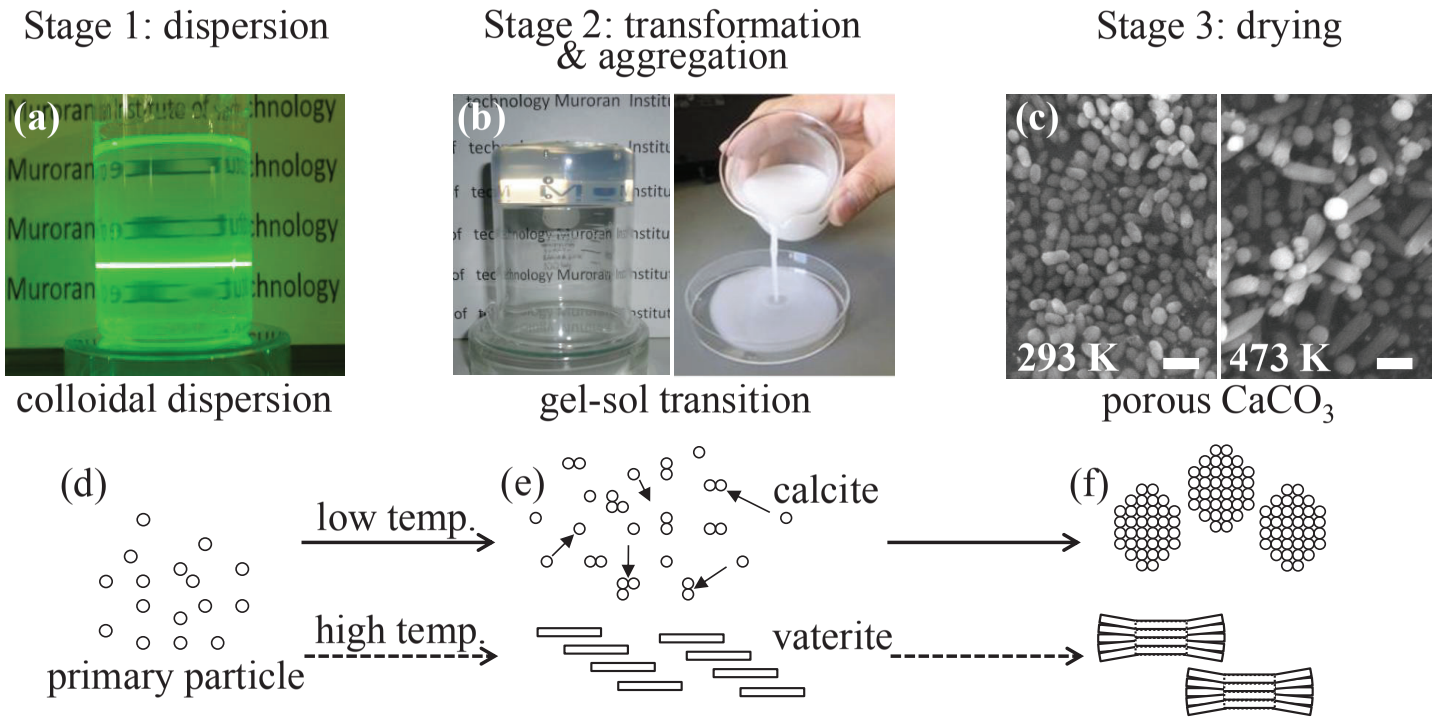
Stage 1: dispersion
Stage 2: transformation & aggregation
Stage 3: drying
(a)
(b)
(c)
293 K
473 K
colloidal dispersion
gel-sol transition
porous $CaCO_3$
(d)
(e)
(f)
low temp.
high temp.
calcite
vaterite
primary particle

Fig. 2

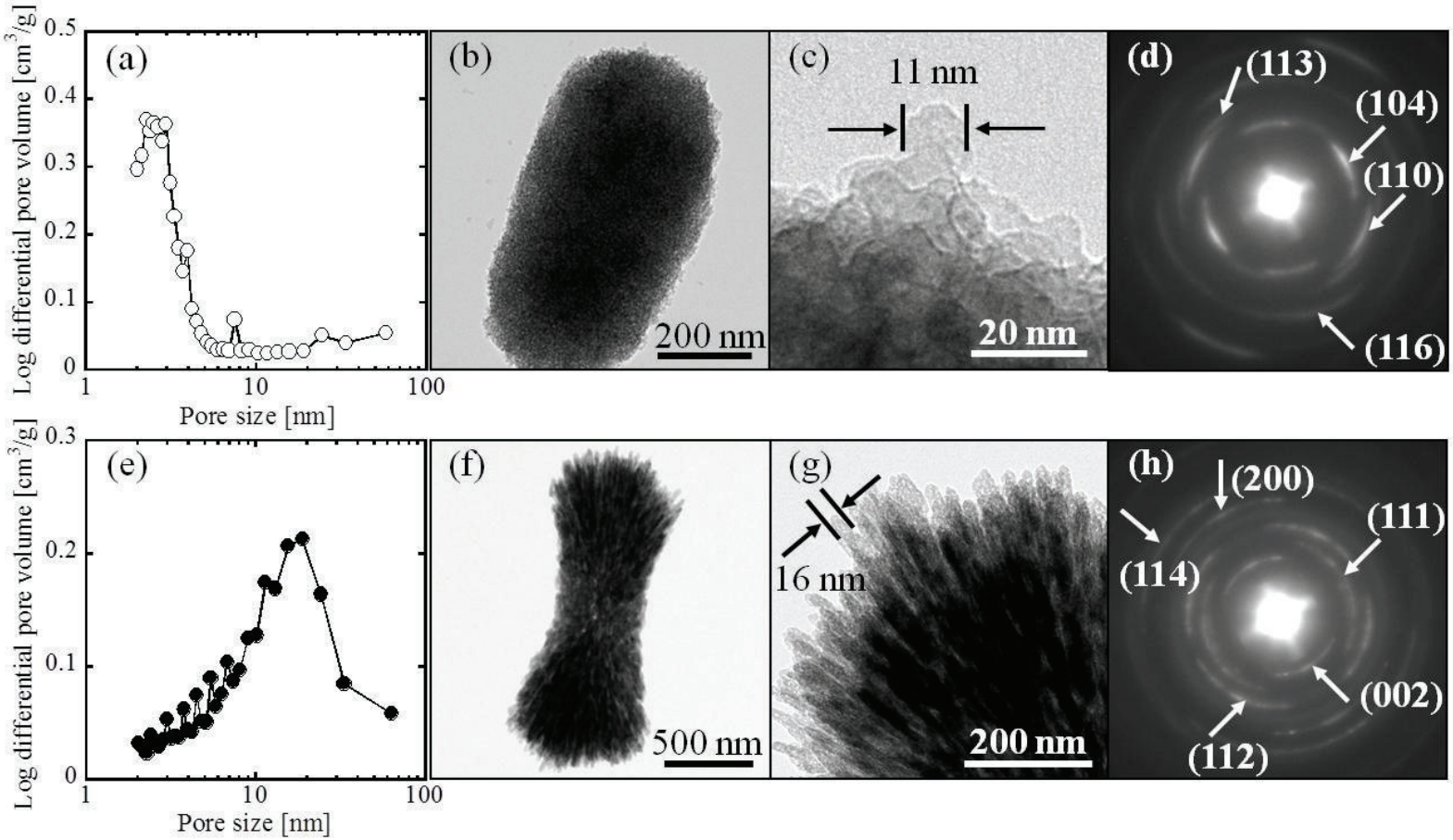
(a)
Log differential pore volume [cm^3/g]
0.5
0.4
0.3
0.2
0.1
0
1
10
100
Pore size [nm]
(b)
200 nm
(c)
11 nm
20 nm
(d)
(113)
(104)
(110)
(116)
(e)
Log differential pore volume [cm^3/g]
0.3
0.2
0.1
0
1
10
100
Pore size [nm]
(f)
500 nm
(g)
16 nm
200 nm
(h)
(200)
(111)
(114)
(002)
(112)

Fig. 3

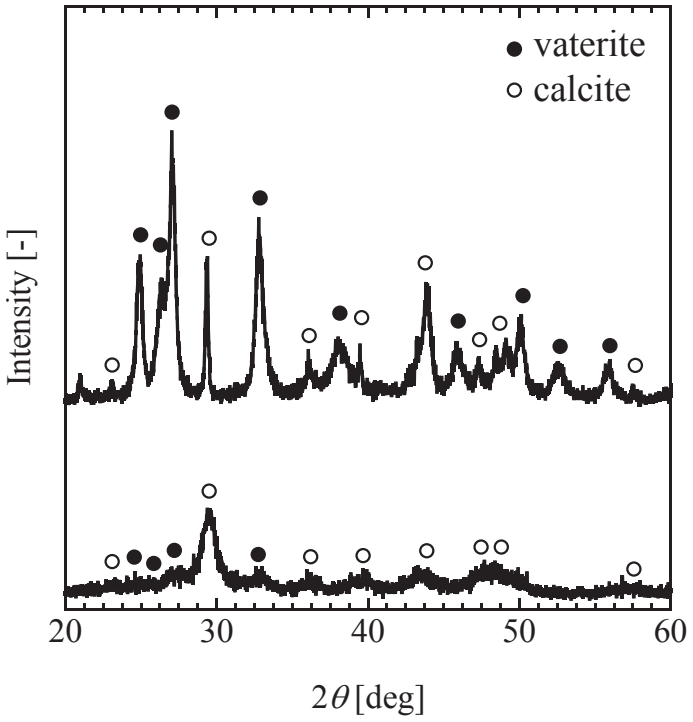

Fig. 4

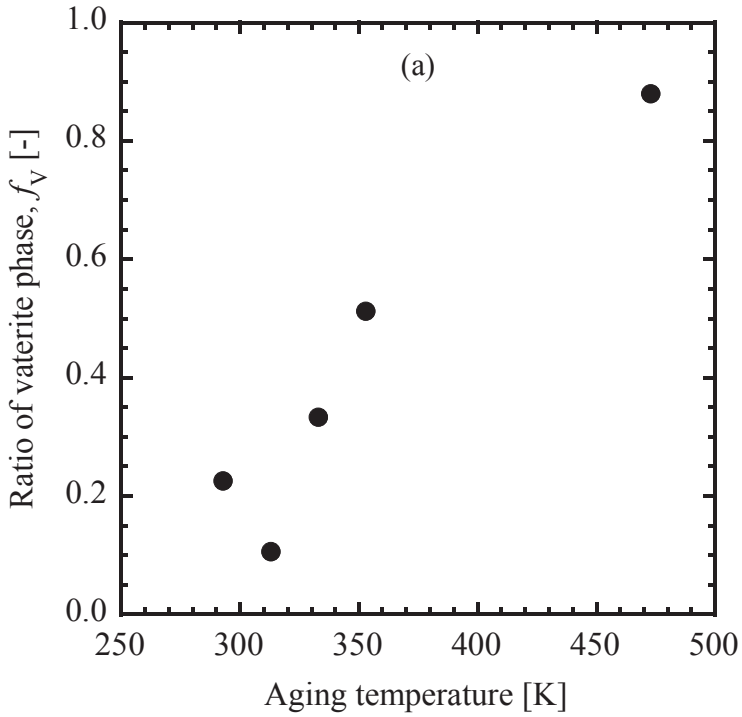
(a)
Ratio of vaterite phase, f_V [-]
1.0
0.8
0.6
0.4
0.2
0.0
250
300
350
400
450
500
Aging temperature [K]

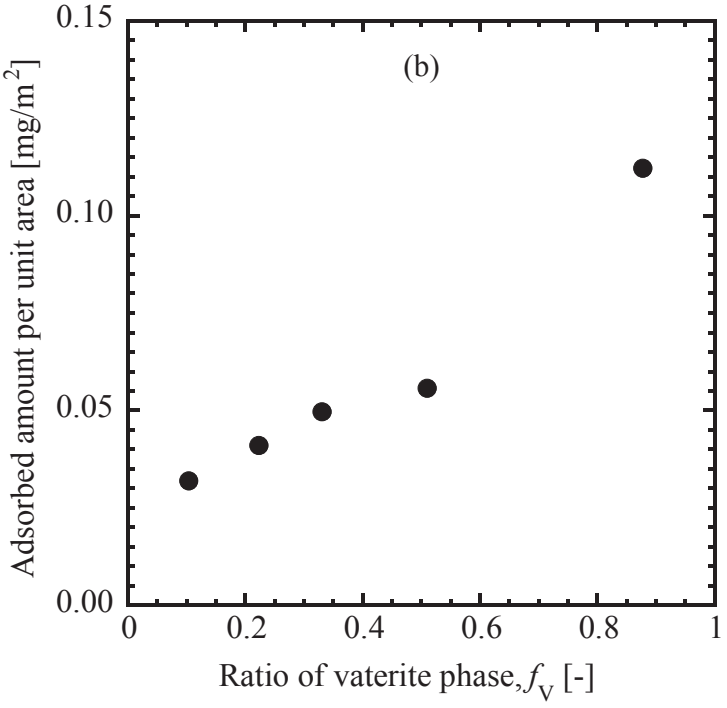
(b)
Adsorbed amount per unit area [mg/m^2]
0.15
0.10
0.05
0.00
0
0.2
0.4
0.6
0.8
1
Ratio of vaterite phase, f_V [-]

Table

Table 1 Characterization results of porous calcium carbonate

Aging temperature [K]	f_V[1] [-]	Particle size[2] [μm]	BET specific surface area [m^2/g]	Total pore volume [cm^3/g]	Mean pore size [nm]
293	0.22	major axis: 0.63±0.07 minor axis: 0.33±0.04	207.3±9.8	0.454±0.034	8.8±0.6
473	0.88	major axis: 1.45±0.36 minor axis: 0.40±0.07	65.1±10.1	0.317±0.020	19.9±2.6

[1]f_V denotes the ratio of vaterite to calcite calculated from XRD intensity.

[2]Measured 100 particles from each SEM image.